JOURNAL OF APPLIED ELECTROCHEMISTRY **27** (1997) 890–901

Effect of contact resistance between particles on the current distribution in a packed bed electrode

J. O'M. BOCKRIS, J. KIM

Surface Electrochemistry Laboratory, Department of Chemistry, Texas A&M University, College Station, TX 77843, USA

Received 16 July 1996; revised 15 November 1996

A microscopic, modelistic approach was carried out to elucidate the electrochemical reduction of a nuclear waste solution in a packed bed electrode. The interfacial surface reactions within the packed bed were taken into account and the particle–particle contact resistance through oxide films was found to be big enough to effect the potential distribution throughout the bed. On the basis of equations developed here, the contribution of the resistance of the oxide film to the potential and current distribution throughout the bed was compared with the macroscopic homogeneous approach.

List of symbols

a cross-sectional area of packed bed electrode
A specific area of packed bed electrode per unit volume
b radius of contact area between two adjacent particles
C concentration
d thickness of surface film or diameter of particle
D diffusion coefficient
F Faraday constant or force
g gravitational acceleration constant
i_o exchange current density
I current
L bed length of packed bed electrode
n number of electrons
N_p number of particles in a slab
N_s number of slabs in a packed bed electrode
p_m mean yield pressure
q charge
r particle radius
R resistance or gas constant
S apparent contact area
S_o real contact area
T absolute temperature
u flow rate
Y Young's modulus

Greek letters
α transfer coefficient
δ diffusion layer thickness
ε_o vacuum permittivity
ε voidage or dielectric constant
η overpotential
μ viscosity
ρ density
σ conductivity

Subscripts
ct contact resistance
c constriction resistance
f film
m electrode
s electrolyte

1. Introduction

Three-dimensional electrodes are attractive for industrial applications such as metal ion removal from dilute solutions [1–3], electroorganic reactions [4–7], water splitting [8, 9], bromide recovery from brine solution [10], synthesis of hydrogen peroxide [11] etc. Three-dimensional electrodes provide an extensive interfacial surface area and involve forced convection by means of flow through the electrodes.

Chu *et al*. [12] were the first to establish an analytic equation for current as a function of time, flow rate, and bed length, when the reaction is mass transfer controlled. A two-dimensional treatment for a packed-bed electrode, in which the direction of solution flow is perpendicular to the direction of current, was authored by Alkire and Ng [13] in 1974 with cylindrical coordinates for practical applications. Kreysa and Heitz [14] established an empirical law which can be used to find the effective length of the electrode. Fedkiw and Newman [15] introduced a periodically constricted model for mass transfer phenomena in a packed-bed electrode though the results were not significantly different from those obtained with homogeneous models [16]. Lyke and Langer [17] in 1991 illustrated the effect of ohmic drop in a packed-bed electrode when Tafel kinetics are followed. In the same year, the effect of gas bubbles formed in the three-dimensional electrode was studied [18] for application of the electrode to hydrogen evolution reaction [9]. A 'macro' or 'homogeneous' model has been employed usually. The electrode

0021-891X

phase is isotropic and homogeneous and of uniform porosity. Ohm's law is thus applied in both the electrode and electrolyte phases [19].

A 'micro' model in which each particle is taken to exhibit a 'localized' variation of potential through the electrode and electrolyte phases is proposed. A contact resistance between particles of the bed (corresponding to the surface condition of Ni at pH 14 and varying with height in the electrode) is taken into account. The treatment in this paper differs from that in the famous paper of Newman and Tobias [20]. In that paper, the type of treatment is continuous and homogeneous. The model of the present paper is discrete and heterogeneous, especially in the treatment of the particle electrodes. This treatment is more realistic than that of a continuum and allows for structural details, such as the resistance between the particles caused by oxide films, to be taken into account.

2. Experimental details

A schematic of the electrochemical cell for the packed-bed electrode is shown in Fig. 1. On a fritted glass (ASTM 145–175 μm) a current collector (Ni gauze, Electrosynthesis Co.) on which the electrode particles rested, was placed. The cathode compartment was connected through a Nafion® 117 film to the anodic compartment which has a counter-electrode (Pt gauze). The electrolyte in the anodic compartment was stagnant while the electrolyte in the cathodic compartment was kept flowing through the bed electrodes. The reference electrode used was the saturated calomel electrode (Fisher Scientific Co.) of which the standard potential is +0.24 V in the normal hydrogen scale.

The bed material was Ni (99.9%, Johnson–Matthey) which was grouped into five particle size ranges ($50-75\ \mu$m, $75-100\ \mu$m, $125-250\ \mu$m, $250-370\ \mu$m and $430-590\ \mu$m radius) with appropriate sieves (Gilson Company Inc.). Before each experiment, the Ni particles were washed with 30% HNO_3 and rinsed with distilled water thoroughly, then packed into the cell. The apparent cross-sectional area of the bed electrode was $1.3 \times 10^{-3}\ m^2$. The length of the bed in the cell (usually about 0.02 m) was varied from 0.01 to 0.06 m to study the effect of the length of the bed on the rate of the reduction of nitrate and nitrite.

The electrolyte in the cathodic compartment was circulated by means of a pump (March Mfg. Inc.). The flow rate was controlled by adjusting the inlet of the pump and was measured with a flow meter (Cole–Parmer Co.) the upper limit of which was $8.3\times 10^{-6}\ m^3 s^{-1}$.

The chemicals for preparing the electrolytic solutions were NaOH (97%, EM Science), $NaNO_3$ (98%, Aldrich), $NaNO_2$ (97%, Aldrich) and sodium tetranitronitrosyl ruthenate (II), $Na_2[RuNO(NO_2)_4OH]\text{-}2H_2O$, which was used because it contains Ru in a form found in low level nuclear waste. The electrolytic solution in the electrochemical cell was purged for 1 h with Ar (99.998%) before each run to remove oxygen in the solution circulated by the pump.

An AMEL potentiostat (model 550) was used to control the potential of the working electrodes, and current was obtained by means of an AMEL inter-

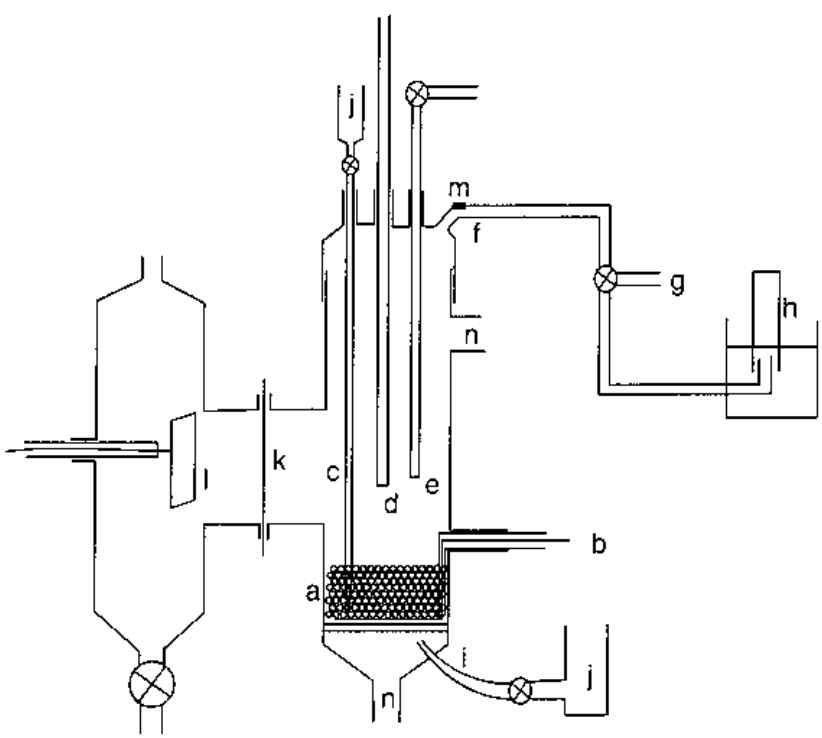

Fig. 1. Schematic for the laboratory scale packed bed electrode. Key: (a) bed of particles, (b) current collector;, (c) Luggin capillary, (d) thermometer, (e) purging gas in, (f) gas out, (g) bubbler, (h) gas collector, (i) Luggin capillary, (j) reference electrode, (k) Nafion® film, (l) counter electrode, (m) septum for gas analysis and (n) solution flow in or flow out.

face (model 560). The currents were recorded by means of a Hewlett Packard 7044B X–Y recorder or a Phillips 8271 X–Y–t recorder.

3. Experimental results

3.1. *Activation-controlled reaction*

The reduction of a solution containing 1.95 M $NaNO_3$, 0.66 M $NaNO_2$, and 1.33 M NaOH at Ni was found to be activation controlled at an applied potential of −0.8 V vs NHE [21]. Measurements, in which a number of parameter (particle size, flow rate, bed height) were varied, were carried out during the reduction of nitrate and nitrite to ammonia and nitrogen.

The currents for the reduction of the electrolytic solution containing 1.95 M $NaNO_3$, 0.66 M $NaNO_2$, and 1.33 M NaOH at −0.8 V were measured as a function of the average radius of the Ni particles in the packed bed electrodes (Fig. 2). The cross sectional area of the bed was 1.3×10^{-3} m^2 and the length of the bed was 0.02 m. As the average radius increases, the current for the reduction of the solution decreases regardless of the flow rate of the solution through the bed. This is because the apparent area per unit volume of the bed decreases as the particle radius increases. In the particle radii range 63–500 μm the current is approximately inversely proportional to the particle radius.

With a constant average particle radius, the effect of the flow rate on the rate of the reduction of an electrolytic solution containing 1.95 M $NaNO_3$, 0.66 M $NaNO_2$, and 1.33M NaOH at −0.8 V at a Ni particle packed bed electrode is shown in Fig. 3. The rate of reduction of the solution at the packed bed electrode remains independent of the flow rate. This result confirms that reduction in a solution containing 1.95 M $NaNO_3$, 0.66 M $NaNO_2$, and 1.33 M NaOH is an activation control reaction.

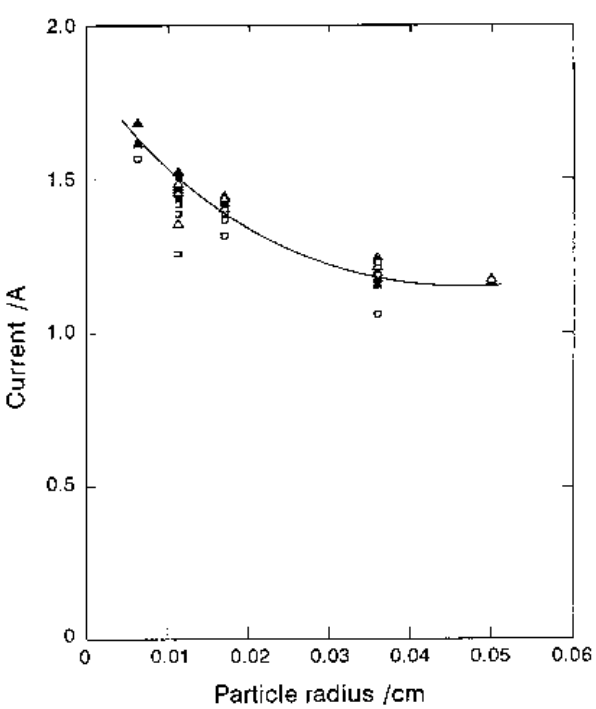

Fig. 2. Total current for the reduction of a solution containing 1.95 M $NaNO_3$, 0.66 M $NaNO_2$, and 1.33 M NaOH at −0.8 V vs NHE at a packed bed electrode as a function of particle radius. $a = 1.3 \times 10^{-3}$ m^2; $L = 0.02$ m. Flow rate, u: (□) 50, (■) 100, (△) 200 and (▲) 400 cm^3 min^{-1}.

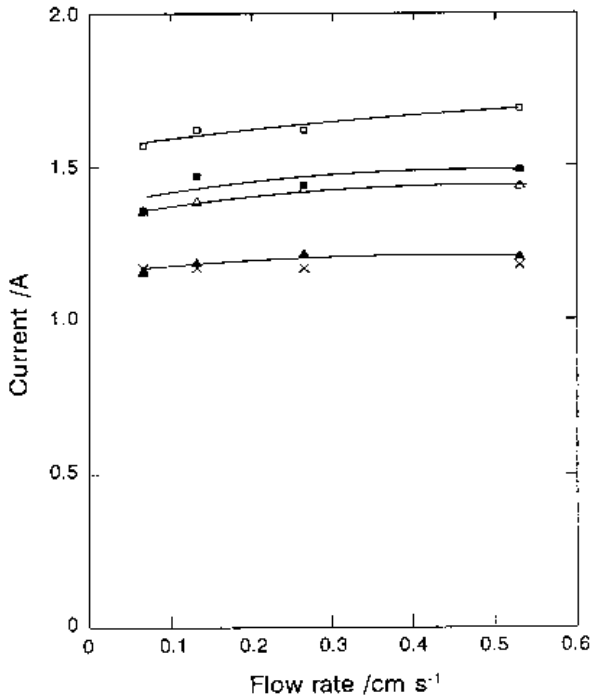

Fig. 3. Total current for the reduction of a solution containing 1.95 M $NaNO_3$, 0.66 M $NaNO_2$, and 1.33 M NaOH at −0.8 V vs NHE at a packed bed electrode as a function of flow rate. $a = 1.3 \times 10^{-3}$ m^2; $L = 0.02$ m. Key: (□) 0.0063, (■) 0.0113, (△) 0.017, (▲) 0.036 and (X) 0.05 cm.

Figure 4 shows the effect of the length of the bed on the rate of the reduction the electrolytic solution containing 1.95 M $NaNO_3$, 0.66 M $NaNO_2$, and 1.33 M NaOH at −0.8 V at a packed bed electrode. The particles were spherical and the average radius, r_{av}, was 110 μm. The cross sectional area of the bed was 1.3×10^{-3} m^2. At a packed-bed electrode, the total current for the reduction of the solution was found to increase with the length of the bed and then reach a limit at an unexpectedly large value of 4×10^{-2} m.

3.2. *Diffusion-controlled reaction*

The reduction of the Ru complex was found to be a diffusion controlled reaction at a Ni electrode [21]. Thus, parametric studies for the diffusion controlled reaction were carried out with variation of the flow rate and the bed length at a Ni particle ($r_{av} = 110$ μm) packed bed electrode.

The current for the reduction of a solution containing 0.4 mM $Na_2[RuNO(NO_2)_4OH]2H_2O$, 1.95 M $NaNO_3$, 0.66 M $NaNO_2$, and 1.33 M NaOH at −0.6 V vs NHE was measured as a function of the flow rate of the solution through a packed bed electrode of which the cross-sectional area was 1.3×10^{-3} m^2 and the length was 0.02 m (Fig. 5). The currents were

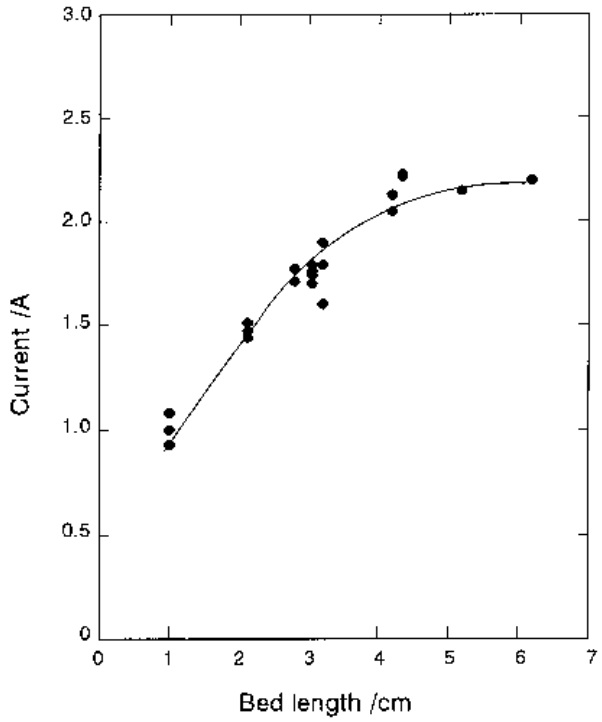

Fig. 4. Total current for the reduction of a solution containing 1.95 M $NaNO_3$, 0.66 M $NaNO_2$, and 1.33 M NaOH at −0.8 V vs NHE at a packed bed electrode as a function of bed length. $a = 1.3 \times 10^{-3}$ m^2; $L = 0.02$ m; $r = 1.1 \times 10^{-4}$ m; $u = 1.66 \times 10^{-6}$ m^{3}s^{-1}.

background-corrected by subtracting the current in a solution containing 1.95 M $NaNO_3$, 0.66 M $NaNO_2$, and 1.33 M NaOH at −0.6 V vs NHE. As the flow rate increases, the current also increases.

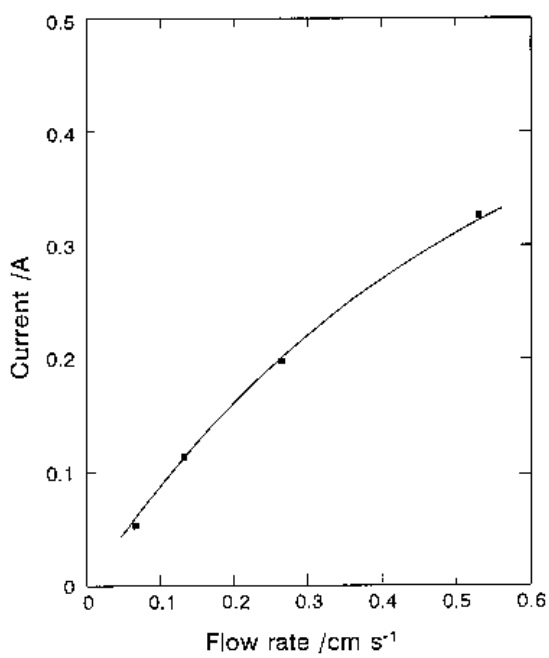

Fig. 5. Total current for the reduction of a solution containing 0.4 mM $Na_2[RuNO(NO_2)_4OH]2H_2O$, 1.95 M $NaNO_3$, 0.66 M $NaNO_2$, and 1.33 M NaOH at −0.6 V vs NHE at a packed bed electrode as a function of flow rate. $a = 1.3 \times 10^{-3}$ m^2; $L = 0.02$ m; $r = 1.1 \times 10^{-4}$m.

Figure 6 shows the effect of the length of the bed on the rate of the reduction the electrolytic solution containing 0.4 mM $Na_2[RuNO(NO_2)_4OH]2H_2O$, 1.95 M $NaNO_3$, 0.66 M $NaNO_2$, and 1.33 M NaOH at −0.6 V at the Ni packed bed electrode. The particles were spherical and again $r_{av} = 1.1 \times 10^{-4}$ m. The cross sectional area of the bed was 1.3×10^{-3} m^2. The current reached a limit at about 0.03 m.

4. Model development

A mathematical approach to a packed bed electrode will be given using the following assumptions:

(i) The electrochemical reaction at a point in the bed is subject to the normal electrode kinetic equation for activation or diffusion control, according to conditions.
(ii) The whole surface of the spherical particle electrode is effective (see below).
(iii) The potential in the metal phase suffers particle-particle contact resistance consisting of both constriction resistance and film contact resistance.
(iv) The ohmic drop through both the solution phase and the metal-metal contacts is the origin of the variation of overpotential with distance. The contact resistance is a function of depth in the bed.
(v) Any current flowing perpendicular to the direction of flow is neglected.

4.1. *Selection of simple hexagonal packing*

The voidage of a randomly packed bed is 0.4 [22]. Among possible packing arrays, the simple hexagonal array has a voidage of 0.396 while voidages for a simple cubic array and a face centered closest array are 0.476 and 0.259, respectively. A simple hexagonal array was chosen as a model for the packed bed electrode. In this structure, the spherical particles are packed as shown in Fig. 7. The bed is assumed to be a

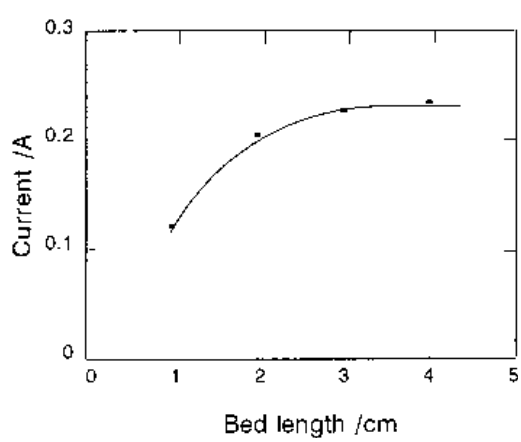

Fig. 6. Total current for the reduction of a solution containing 0.4 mM $Na_2[RuNO(NO_2)_4OH]2H_2O$, 1.95 M $NaNO_3$, 0.66 M $NaNO_2$, and 1.33 M NaOH at −0.6 V vs NHE at a packed bed electrode as a function of bed length. $a = 1.3 \times 10^{-3}$ m^2; $L = 0.02$ m; $r = 1.1 \times 10^{-4}$ m.

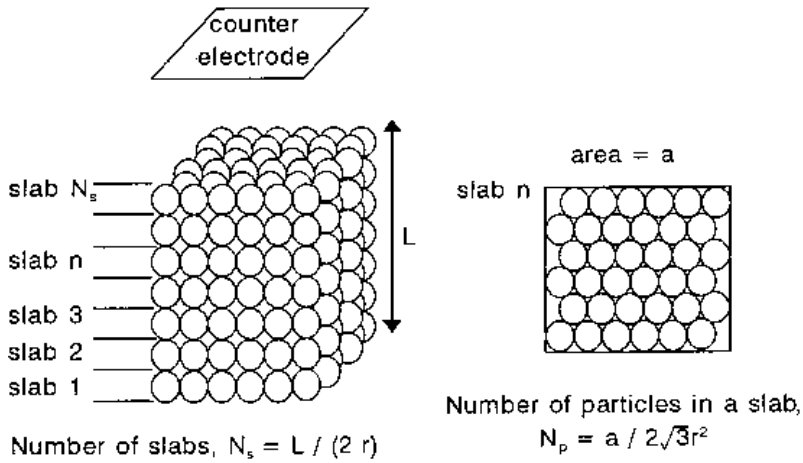

Fig. 7. A simple hexagonal packing structure with uniform spherical particles.

pile of slabs. The number of slabs (N_S) in a packed bed electrode is $L/2r$ where L is the bed length and r is the radius of a spherical particle. The number of particles (N_P) in each slab is $a/r^2 2\sqrt{3}$ where a is the cross-sectional area of the bed.

4.2. *Current at a slab*

When a spherical particle is placed in a solution as an electrode, under activation control, current through the interface of the spherical particle (I_P) is simply represented* as

$$I_P = 4\pi r^2 i_o \exp\left(-\frac{\alpha\eta_P F}{RT}\right) \tag{1}$$

where r is particle radius, i_o is the exchange current density, a the transfer coefficient and η_P is the overpotential at the particle p.

Since all particles in a given slab have the same overpotential (η_S), the current at a slab (I_S) is expressed as

$$I_s = I_P N_P = 4\pi r^2 \frac{a}{2\sqrt{3}r^2} i_o \exp\left(-\frac{\alpha\eta_s F}{RT}\right) = \frac{2\pi a}{\sqrt{3}} i_o \exp\left(-\frac{\alpha\eta_s F}{RT}\right) \tag{2}$$

When the overpotential at the first slab nearest the current collector (bottom of the bed, Fig. 8) is η_1, the current at this first slab is

$$I_1 = \frac{2\pi a}{\sqrt{3}} i_o \exp\left(-\frac{\alpha\eta_1 F}{RT}\right) \tag{3}$$

Correspondingly, the current at the second slab is described by

$$I_2 = \frac{2\pi a}{\sqrt{3}} i_o \exp\left(-\frac{\alpha\eta_2 F}{RT}\right) \tag{4}$$

* The potential difference between both ends of a sphere is $IR = i\pi r^2 \times 2r/\sigma_S \pi r^2 = 2ir/\sigma_S$. With $i = 10^2\,\mathrm{A\,m^{-2}}$, $r = 10^{-4}$ m, and $\sigma_S = 10\,\Omega^{-1}\,\mathrm{m}^{-1}$, the potential drop is 0.002 V. With the transfer coefficient of 0.33, the current density at the bottom is 97% of the current density at the top. Thus, whole surface is considered to be active.

where η_2 is the overpotential at the second slab. The current at the nth slab is

$$I_n = \frac{2\pi a}{\sqrt{3}} i_o \exp\left(-\frac{\alpha\eta_n F}{RT}\right) \tag{5}$$

and the total current in the bed is obtained from the summation of all currents at the slabs as

$$I_T = \sum_{n=1}^{N_s} I_n = \sum_{n=1}^{N_s} \frac{2\pi a}{\sqrt{3}} i_o \exp\left(-\frac{\alpha\eta_n F}{RT}\right) \tag{6}$$

The ohmic drop through the solution phase makes the overpotential at the top of the bed more cathodic than the overpotential applied at the bottom of the bed. The ohmic drop through the metal phase will decrease (i.e., make less cathodic) the overpotential at the top of the bed. To determine the ohmic drops both through the solution phase and through the metallic phase, one has to determine the currents at both phases as well as the resistance. Figure 8 demonstrates this. Let the current at the first slab (the bottom of the packed bed) be I_1, and the current at the nth slab be I_n. Then, the total current in the packed bed electrode, I_T,

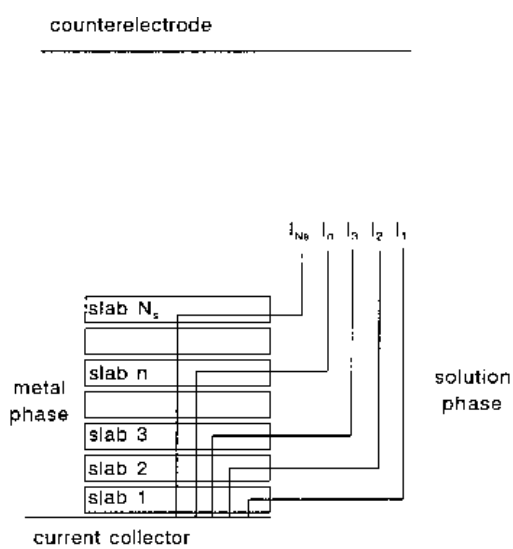

Fig. 8. Schematic of the current at each slab and its contribution to the IR drops in the solution and in the electrode phase.

is $I_1 + I_2 + I_3 + \cdots + I_n + \cdots + I_{Ns}$. The electronic partial current flowing from slab 2 to slab 1 through the metallic phase is $I_T - I_1$ while the ionic partial current flowing from slab 2 to slab 1 through the solution phase is I_1. The electronic partial current flowing from slab 3 to slab 2 through the metallic phase is $I_T - (I_1 + I_2)$ while the ionic partial current flowing past slab 3 to slab 2 through the solution phase is $I_1 + I_2$. Thus, between the $(n-1)$th slab and the nth slab, the current through the solution phase is formulated as $I_1 + I_2 + I_3 + \cdots + I_{n-1}$ while the current through the metallic phase is formulated as $I_T - (I_1 + I_2 + I_3 + \cdots + I_{n-1})$. The difference of the overpotential between the $(n-I)$th slab and the nth slab is thus (see Appendix A)

$$\eta_n = \eta_{n-1} - \sum_{n=1}^{n-1} I_n R_s + \left(I_T - \sum_{n=1}^{n-1} I_n\right) R_{m,n} \quad (7)$$

where R_s and $R_{m,n}$ are the resistance between two adjacent slabs through the solution phase and through the electrode phase, respectively. $R_{m,n}$ is a function of the position of the slab in the bed. The negative sign of the second term on the right side of Equation 7 refers to the cathodic shift of the overpotential as one proceeds in the solution from the bottom to the top of the bed, which makes the overpotential increasingly negative and a positive sign on the third term of the right side refers to the anodic shift of the overpotential which occurs because of the IR drop through the metal as one proceeds from the bottom to the top of the bed.

From Equation 5 which gives the current at the nth slab, the total current can be formulated as

$$I_T = \sum_{n=1}^{N_s} I_n = \frac{2\pi a}{\sqrt{3}} i_o \sum_{n=1}^{N_s} \exp\left[-\frac{\alpha F}{RT}\left(\eta_{n-1} - \sum_{n=1}^{n-1} I_n R_s + \left(I_T - \sum_{n=1}^{n-1} I_n\right) R_{m,n}\right)\right] \quad (8)$$

The above equation can be solved numerically with some reasonable values for a, i_o, α, R_s, $R_{m,n}$, and the overpotential at the bottom, η_1. After some of the necessary parameters are determined below, the solution of the above equation will be shown later.

4.3. *Resistance in the solution phase*

The resistance R_s, through the solution phase in the packed bed electrode must be determined. The resistance between two neighbouring slabs is then expressed as

$$R_s = \frac{2r}{\sigma_s a} = \frac{2r}{\sigma_{s,o}\varepsilon^{1.5} a} \quad (9)$$

where r is the radius of the particles, $\sigma_{s,o}$ is the conductivity of the solution in a pure solution state, ε is the voidage of the packed bed, and a is the cross-sectional area of the packed bed electrode. The conductivity of a solution containing 1.95 M $NaNO_3$, 0.66 M $NaNO_2$ and 1.33 M NaOH was calculated to be $40\,\Omega^{-1}m^{-1}$ based on values given as the conductivities of 1.95 M $NaNO_3$, 0.66 M $NaNO_2$, and 1.33 M NaOH are 12.36, 6.08 and $22.4\,\Omega^{-1}\,m^{-1}$, respectively [23]. The conductivity of the solution was measured to be $0.32\,\Omega^{-1}m^{-1}$, the 20% deviation arising from the interaction between solute ions. The conductivity of the solution phase [24] in a packed bed is $32\,\Omega^{-1}m^{-1} \times (0.4)^{1.5} = 8\Omega^{-1}m^{-1}$ when the voidage for particles of radius 110 μm of the simple hexagonal array is considered. The voidage (ε) is reported to be a function of particle size [25] according to the relation

$$\varepsilon = 0.361 \times (2r)^{-0.038} \quad (10)$$

The conductivity of the solution phase is thus slightly changed with a variation in the particle radius.

4.4. *Resistance in the electrode phase*

When two spherical particles are pressed against each other with a certain force, F, the apparent contact area, S, assuming ideal smoothness of the contact area, is obtained from [26]

$$S = 3.87(Fr/Y)^{2/3} \quad (11)$$

where r is the particle radius and Y Young's modulus. When two particles contact each other, the current passes through a contact area which is much less then the cross-sectional area of the particle. The contact area, S_o, is then [26]

$$S_o = F/p_m \quad (12)$$

where F is the force acting on the particle and p_m is the mean yield pressure of the asperities and is given by $p_m = cM$, where M is the stress at the elastic limit of the deformed metal at the tip of the asperities. The factor c depends on the shape and the size of the surface irregularities. The parameter c, has a value of about 3 for usual cases (e.g., steel ball, copper sphere etc.) [26]. The elastic limit is assumed to be reached at a strain of 0.5%. From stress–strain curve, $\Delta L/L$ = stress/Y, the stress at the elastic limit for Ni is $0.005 \times 2 \times 10^{11} = 10^9\,N\,m^{-1}$ and the mean yield pressure is $3 \times 10^9\,N\,m^{-2}$. This kind of restriction against the flow of current was introduced as the 'constriction resistance' by Holm [27]. The resistance by a metal–metal contact consists of the constriction resistance, R_c, and the film resistance, R_f at the surface, if a film exists there, as

$$R_{ct} = R_c + R_f = \frac{1}{2\sigma_{m,o} b} + \frac{2d}{\sigma_f \pi b^2} \quad (13)$$

where d is the thickness of surface film, $\sigma_{m,o}$ and σ_f are the conductivities of the pure metallic phase and of the surface film, respectively, and b is the radius of the contact area between two particles. Since there are N_p spherical particles in one slab, the resistance, R_m, from one slab to the next slab through the particle-particle contact is R_{ct}/N_p when the contact resistances are considered to be connected in parallel between two adjacent slabs. Thus,

$$R_m = \frac{R_{ct}}{N_p} = \frac{r^2\sqrt{3}}{\sigma_{m,o} a\ b} + \frac{4\sqrt{3}dr^2}{\sigma_f\ \pi\ a\ b^2} \qquad (14)$$

where r is the particle radius and a is the bed cross-sectional area.

In pure Ni, the electrical conductivity is $1.47 \times 10^7\ \Omega^{-1}\,m^{-1}$. When the particle–particle contact is purely metallic, the contact resistance is too small to be taken into account. However, from the Pourbaix diagram [28] of Ni, Ni is covered with a layer of hydroxide/oxide in a solution of pH 14 in the potential region from −0.8 to 0.0 V vs NHE. In support of this, a broad anodic peak corresponding to anodic nickel oxidation in alkaline solution has been observed at −0.5 V vs NHE in 1 M KOH [29], and the oxide film was not reduced unless the potential was made more cathodic than −0.9 V vs NHE. Thus, hydroxide/oxide layer is considered to exist at the Ni particle surfaces in the solution at the potential region employed in this study (i.e., −0.8 V vs NHE).

Bockris *et al.* [30] showed that the thickness of the oxide film on Ni is about 5×10^{-9}m. The conductivity term in the constriction resistance has to be the conductivity of the oxide film, not that of the pure metal, because the radius of the contact area is just 6.9×10^{-9}m [31]. Trasatti and Lodi show tabulated properties for a number of oxides [32]. Typically among these is that for manganese dioxide, where the conductivity varies in the range 10^3 to $10^4\ \Omega^{-1}\,m^{-1}$. However, a passive layer oxide might be expected to have a somewhat greater conductivity value than this because of the nonstoichiometry of the nickel oxide. The value of $3 \times 10^4\ \Omega^{-1}\,m^{-1}$ for the conductivity of the oxide film used in the calculation gave rise to fair agreement with the experimental data[†].

4.5. *Force and contact area*

If the gravitational force is the only force pressing the particles, this force is

$$F_g = \frac{4}{3}\pi r^3 \rho g \qquad (15)$$

where ρ is the particle density and g is the gravitational acceleration constant. When the density of the solution ($1.2 \times 10^3\ kg\,m^{-3}$ for the solution containing 1.95 M $NaNO_3$, 0.66 M $NaNO_2$, and 1.33 M NaOH) is considered, the density of Ni ($8.9 \times 10^3\ kg\,m^{-3}$) is corrected to $7.7 \times 10^3\ kg\,m^{-3}$.

There is a repulsive force between two neighbouring particles due to repulsion between the two surfaces. Bockris and Argade [33] showed that this repulsive force reduced the friction between a metal slider and a metal plate. The repulsive force due to this double layer repulsion was formulated as

$$F_r = \frac{1}{2\varepsilon_o \varepsilon} q^2 (S - S_o) \qquad (16)$$

where ε_o is the vacuum permittivity ($8.85 \times 10^{-12}\ J^{-1}C^2m^{-1}$), ε is the dielectric constant of the solution, q is the charge built up in the double layer, S is the apparent contact area, and S_o is the real contact area. The apparent contact area and the real contact area are obtained from Equations 11 and 12, respectively. The dielectric constant of 80 was taken for the solution. The charge is calculated from the double layer capacitance (about $0.5\ F\,m^{-2}$) and the potential of zero charge (pzc about −0.5 V vs NHE in pH 14 solution [34]) of Ni. Thus, when the potential is −0.8 V vs NHE, the potential difference from the pzc is −0.3 V, thus, $q = 0.5\ F\,m^{-2} \times 0.3\ V = 0.15\ C\,m^{-2}$. The force will be $(0.15\ C\,m^{-2})^2 \times (1.5 \times 10^{-14} m^2 - 1.5 \times 10^{-16} m^2)/(2 \times (8.85 \times 10^{-12}\ J^{-1}C^2m^{-1}) \times 80) = 2.38 \times 10^{-7}\ N$ about a half of the gravitational force.

The overall force of two neighbouring spherical particles pressing each other is thus

$$F = F_g - F_r = \frac{4}{3}\pi r^3 \rho g - \frac{2\pi}{\varepsilon} q^2 (S - S_o) \qquad (17)$$

There are N_s slabs in a packed bed model thus a particle in the first slab from the current collector feels a gravitational force of $(N_s - 1) \times F_g$, and a particle in the second slab feels $(N_s - 2) \times F_g$, and so on. A particle in the nth slab feels a force of

$$F_n = (N_s - n)F_g - F_r \qquad (18)$$

From this force, from Equation 12, the real contact area may be calculated and thus the radius of the real contact area, b, obtained. Then, from Equation 13, the contact resistance was determined with the conductivity of the metal in bulk, and the conductivity and film thickness of a surface film. The force acting on a particle varies with the position of the particle in a packed bed electrode. As one goes down in the bed, the force increases, the contact area increases, and the contact resistance decrease. These conclusions are used in the calculations described below.

4.6. *Correction for the I–E Curves*

One of the assumptions for using the numerical treatment described in the previous section is that the electrochemical reaction follows the Butler-Volmer equation with a single exchange current density and a single transfer coefficient. However, the Tafel plot for the reduction of the solution containing 1.95 M $NaNO_3$, 0.66 M $NaNO_2$, and 1.33 M NaOH was found to have at least two different transfer coefficients in two different potential regions as [21]

$$i = 5.2 \times 10^{-3} \exp(-0.33\eta F/RT)\ A\,m^{-2} \quad \text{when } \eta < -0.645\ V$$

$$i = 3.16 \times 10^{-21} \exp(-2\eta F/RT)\ A\,m^{-2} \quad \text{when } -0.645\ V < \eta < -0.591\ V$$

[†] The existence of an oxide film might be avoided when pure particles with no oxide film are packed in a bed and the cell is filled with the electrolyte. However, the assumption of a purely metal-to-metal contact does not give rise to consistence between the calculations presented here and the experimental results recorded.

The exchange current value of 10^{-21} A m^{-2} is improbable, even though the value came from the phenomenological analysis for planar electrodes with the equilibrium potential for NO_3^-/NH_3. It might be an artifact which is a middle region between the nitrate reduction and $Ni(OH)_2$ reduction. In the region where the nitrate reduction is not significant, the current–potential response was formulated as

$$i = 3.16 \times 10^{-2} \exp(-0.1\,\eta F/RT)\ \mathrm{A\,m^{-2}}$$
$$\text{when } \eta > -0.591\ \mathrm{V}$$

The exchange currents were calculated from the equilibrium potential for the reduction of nitrate to ammonia of −0.085 V vs NHE and the slope of $\log i - \eta$ plot at each region. In the calculation of the current at each slab in the packed bed electrode, one of three equations described above is used according to the potential region considered.

4.7. *Calculation and comparison with experimental data of current in a packed bed electrode*

With other constants known, the total current from Equation 8 can be calculated numerically [31]. Figures 9 to 11 show the log I against η plot, the I against r plot and the I against L plot from the calculations with the constants assumed above and these model calculations were compared with the experimental results. The calculations were in fair agreement with the experimental values.

If the total area of a packed bed electrode is taken to be $4\pi aL/r\sqrt{3}$, where a is the cross sectional area of the bed, L is the length of the bed and r is the radius of the particle, the total current observed would have to be proportional to $1/r$. However, the experimental results (Fig. 10) show that the total current measured was proportional to $r^{-0.1}$. In the calculation, the total current is proportional to which is in good agreement with the experimental data. This relatively low index may be interpreted in terms of the contact resistance which is a function of the radius of the particles. As the radius increases, the weight of the individual particle increases, and the contact resistance decreases, giving rise to an increase in the total current, which is compensated with the decrease of the surface area of a packed bed as the radius of particle increases.

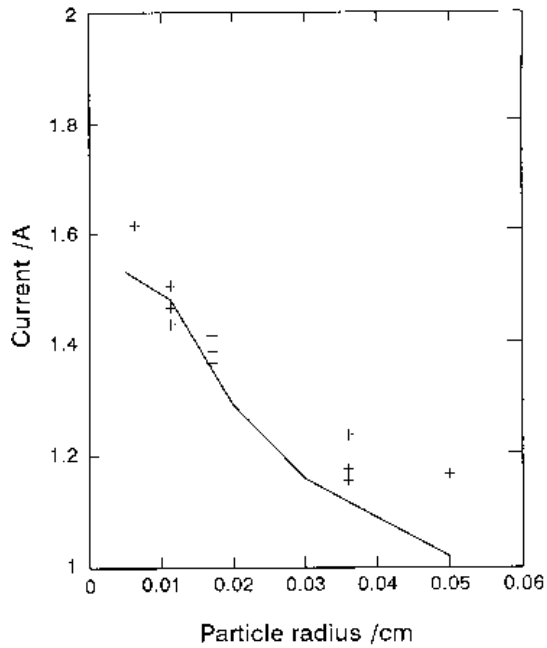

Fig. 10. Calculation of I against r plot for the reduction of a solution containing 1.95 M $NaNO_3$, 0.66 M $NaNO_2$, and 1.33 M NaOH and comparison with experimental values (plots +). $a = 1.3 \times 10^{-3}$ m^2; $L = 0.02$ m

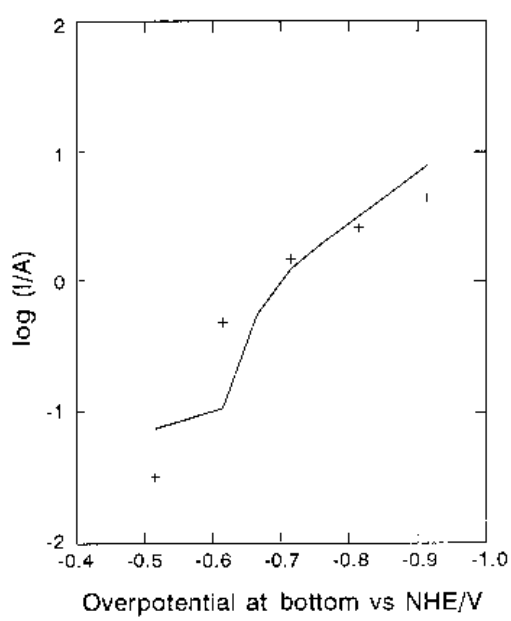

Fig. 9. Calculation of I against η_o plot for the reduction of a solution containing 1.95 M $NaNO_3$, 0.66 M $NaNO_2$, and 1.33 M NaOH and comparison with experimental values (plots +). $a = 1.3 \times 10^{-3}$ m^2; $L = 0.02$ m; $r = 1.1 \times 10^{-4}$ m.

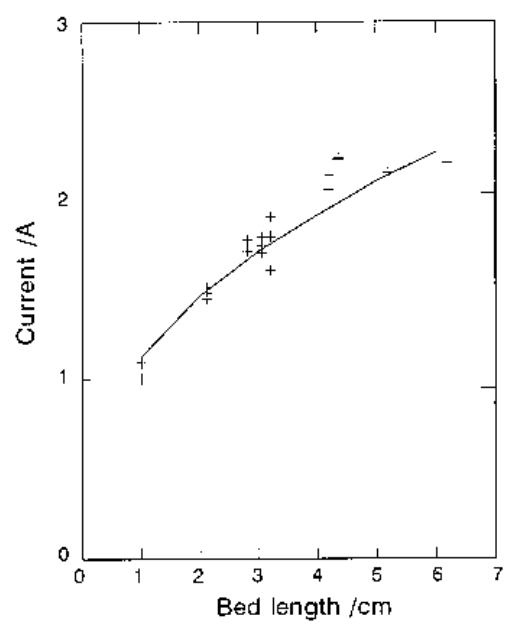

Fig. 11. Calculation of I against L plot for the reduction of a solution containing 1.95 M $NaNO_3$, 0.66 M $NaNO_2$, and 1.33 M NaOH and comparison with experimental values (plots +). $a = 1.3 \times 10^{-3}$ m^2; $r = 1.1 \times 10^{-4}$ m.

The dependence of the total current on the total bed length (Fig. 11) seems much larger than one would expect from the theory of Newman and Tobias [20] so far as the effective depth is concerned. In the absence of an *IR* drop in the metallic phase, the effective length, defined as a depth at which the local interfacial current density is one hundredth of the total current density, would be about 0.5 cm. However, experimentally, in the Ni-alkaline solution cell, the total current at the packed bed electrode increases as the bed length increases to 4 cm. Many different models were tried to explain the anomalously high value of the effective length. The only model in accord with observation was that in which the total current is related to the contact resistances between particles which vary as the bed length changes. The increase in total current with increase in bed length is interpreted in terms of the contact resistance. As the total bed length increases, the force acting on the particles near to the current collector increases, the contact resistance decreases, and the total current increases. Even though a clear cut effective bed length was not found in the simulation, the latter gave a fair agreement with the experimental observations (+'s in Fig. 11).

4.8. *Overpotential and current distribution*

The calculated distributions of the overpotential and current as a function of position are shown in Fig. 12. The distributions shown there differ from those expected on the conventional view which considers the metal phase to be equipotential [19] or the conductivity of metal phase to be a fraction of the bulk metal conductivity ($\sigma_m = \sigma_m^o(1-\varepsilon)^{1.5}$) and thus the current distribution would be localized to the top of the bed only. However, when a contact resistance exists at the particle-particle contact it has a significant effect on the potential distribution through the metallic phase. The calculation shows (Fig. 12) that the effective regions in the bed are located both at the top of the bed (i.e., the nearest portion to the counterelectrode) and at the bottom of the bed (i.e., the nearest portion to the current collector). This is in contrast to the usual analysis in which the current is significant only at the top of the bed.

4.9. *Mass transfer control*

Electrochemical reduction of 0.4 mM $Na_2[RuNO(NO_2)_4OH]2H_2O$ in a solution containing 1.95 M $NaNO_3$, 0.66 M $NaNO_2$, and 1.33 M NaOH at Ni particles ($\tau_{av} = 1.1 \times 10^{-4}$ m) in a packed bed ($a = 1.3 \times 10^{-3} m^2$) electrode at -0.6 V vs NHE (applied to the bottom of the bed) showed that the total current increases as the flow rate increases, reaching an asymptote at large bed lengths (Figs 5 and 6). The reduction of the ruthenium complex was found to be diffusion controlled [21]. It may be argued that some part of the packed bed would be out

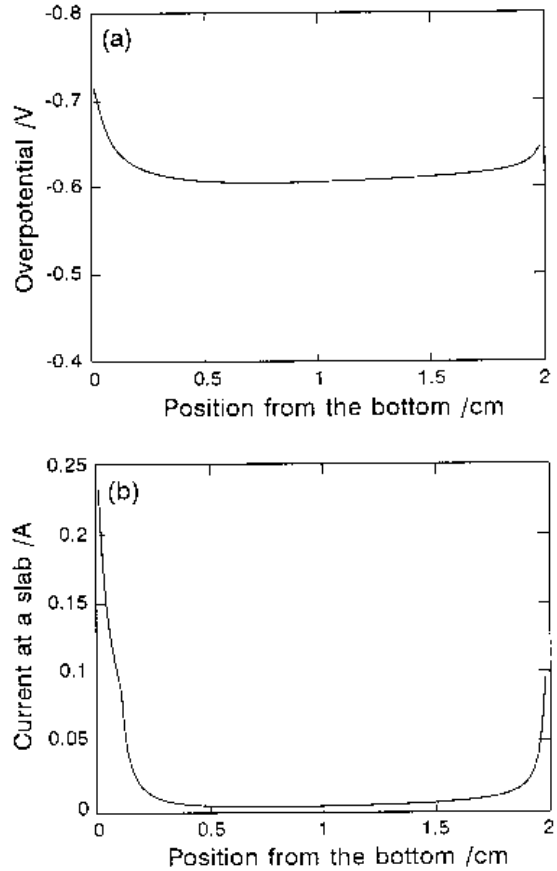

Fig. 12. (a) Overpotential and (b) current at a slab in a packed bed electrode with the overpotential at the bottom of tile bed −0.715 V. $a = 1.3 \times 10^{-3}$ m^2; $L = 0.02$ m; $r = 1.1 \times 10^{-4}$ m.

of the mass-transfer controlled region. However, the potential was applied at the bottom of the packed bed so that the actual interfacial potential at the top would be more cathodic than at the bottom. Thus, all reaction at the packed bed was considered to be under mass transfer control. Chu *et al.* [12] had already established an analytical equation for the current under mass transfer control at a packed bed electrode as a function of flow rate, particle size, bed length, and concentration. In this Section, an approach similar to that for the activation controlled case is pursued.

In a packed bed electrode, the limiting current density at a certain slab m is

$$i_m = \frac{nFDC_m}{\delta_{PBE}} \tag{19}$$

where C_m is the concentration of the electroactive species at the slab m and δ_{PBE} is the diffusion layer thickness at a packed bed electrode. In the above equation, the diffusion layer thickness and the concentration term have to be evaluated to determine the current at the mth slab.

The diffusion layer thickness is not easy to calculate because of the irregularity of the voids in the packed bed electrode. An empirical expression for the diffusion layer thickness is [35]

$$\delta = d\left[2 + 1.1\left(\frac{\mu}{\rho D}\right)^{1/3}\left(\frac{u\rho d}{\mu}\right)^{0.6}\right]^{-1} \qquad (20)$$

where d is the diameter of the particle, μ is the viscosity of the solution, u is the flow rate, and ρ is the density of the solution. When the flow rate is $2.65 \times 10^{-3}\,\mathrm{m\,s^{-1}}$ (with $a = 1.3 \times 10^{-3}\mathrm{m}^2$), the diffusion layer thickness is calculated to be 1.95×10^{-5}m with the density of the solution as $1.2 \times 10^3\,\mathrm{kg\,m^{-3}}$ and the viscosity of the solution as 1.5 centipoise ($1.5 \times 10^{-3}\mathrm{kg\,m^{-1}\,s^{-1}}$).

From the mass action law, $I = nFau\Delta C/\varepsilon$, where ε is introduced because the average flow rate in a bed [12] is u/ε, the concentration at the slab m, C_m, is described as

$$C_m = C_{m-1} - \varepsilon\frac{I_{m+1}}{nFau} \qquad (21)$$

where C_{m+1} is the concentration at the $(m+1)$th slab, n is the number of electrons, F is Faraday's constant. Since the solution flows downward and the index number counts upward, the concentration at the mth slab is lower than that at $(m+1)$th slab (see Fig. 8). The concentration for any slab is

$$C_m = C_{\mathrm{L}} - \varepsilon\frac{I_{\mathrm{T}} - \sum_{n=1}^{m} I_n}{nFau} \qquad (22)$$

where C_{L} is the concentration at the top of the bed or the input concentration. The above equation reveals that the concentration at any slab in the bed can be represented as a function of current and flow rate. Then, Equation 19 is rearranged to be

$$i_m = \frac{nFD}{\delta_{\mathrm{PBE}}}\left(C_{\mathrm{L}} - \varepsilon\frac{I_{\mathrm{T}} - \sum_{n=1}^{m} I_n}{nFau}\right) \qquad (23)$$

When a simple hexagonal packing structure (Fig. 7) is adapted, the current at the mth slab is

$$I_m = 4\pi r^2 N_{\mathrm{p}} i_m = \frac{2\pi anFD}{\sqrt{3}\ \delta_{\mathrm{PBE}}}\left(C_{\mathrm{L}} - \varepsilon\frac{I_{\mathrm{T}} - \sum_{n=1}^{m} I_n}{nFau}\right) \qquad (24)$$

The total current at the bed is then

$$I_{\mathrm{T}} = \sum_{m=1}^{L/2r} I_m = \frac{2\pi anFD}{\sqrt{3}\ \delta_{\mathrm{PBE}}}\sum_{m=1}^{L/2r}\left(C_{\mathrm{L}} - \varepsilon\frac{I_{\mathrm{T}} - \sum_{n=1}^{m} I_n}{nFau}\right) \qquad (25)$$

and is determined by numerical iteration with the constants of a, n, D, δ_{PBE}, C_{L} and u. Equation 25 can be transformed to the generalized expression of Chu *et al.* for the current in a packed bed electrode under mass transfer control (see Appendix B).

With $a = 1.3 \times 10^{-3}\mathrm{m}^2$, $n = 2$, $D = 0.5 \times 10^{-9}$ $\mathrm{m^2 s^{-1}}$, $\varepsilon = 0.4$ and $r_{\mathrm{av}} = 1.1 \times 10^{-4}$ m, the total current at the packed bed electrode for the reduction of 0.4 mM $Na_2[RuNO(NO_2)_4OH]2H_2O$ in a solution containing 1.95 M $NaNO_3$, 0.66 M $NaNO_2$, and 1.33 M NaOH (at −0.6 V vs NHE applied at the bottom of the bed) was calculated and compared to the experimental results in Figs 13 and 14 as a function of the bed length and the flow rate, respectively. The calculation is in a fair agreement with the experimental value.

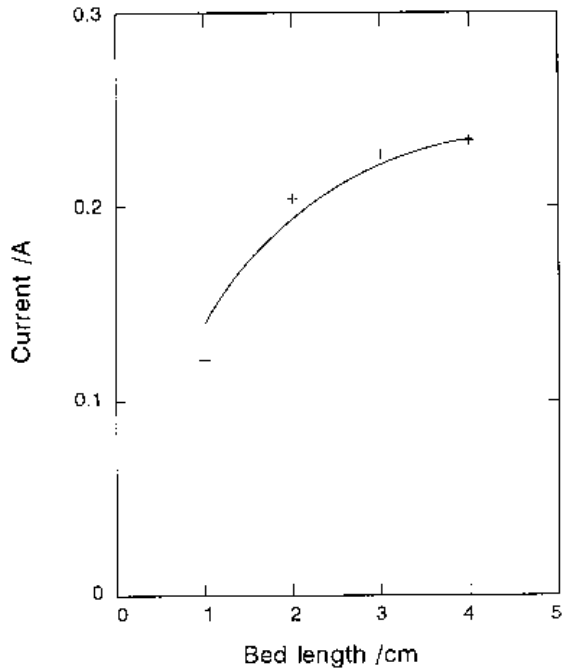

Fig. 13. Calculation of I against L plot for the reduction of a solution containing 0.4 mM $Na_2[RuNO(NO_2)_4OH]2H_2O$, 1.95 M $NaNO_3$, 0.66 M $NaNO_2$, and 1.33 M NaOH at −0.6 V vs NHE and comparison with experimental values (plots +). $a = 1.3 \times 10^{-3}$ m^2; $u = 3.3 \times 10^{-6}$ m^{3}s^{-1}.

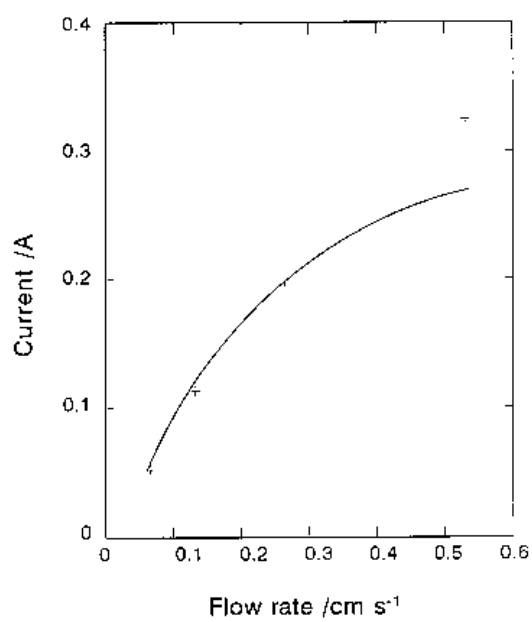

Fig. 14. Calculation of I against u plot for the reduction of a solution containing 0.4 mM $Na_2[RuNO(NO_2)_4OH]2H_2O$, 1.95 M $NaNO_3$, 0.66 M $NaNO_2$, and 1.33 M NaOH at −0.6 V vs NHE and comparison with experimental values (plots +). $a = 1.3 \times 10^{-3}$ m^2; $L = 0.02$ m; $r = 1.1 \times 10^{-4}$ m.

4.10. *Comparison of heterogeneous (or microscopic) and homogeneous (or macroscopic) approaches*

The prediction of overpotential and current distribution in a packed bed electrode have already been carried out elsewhere, based on treating the solution and the electrode phases as two continua [20, 36]. When the particles are small enough, the two approaches, homogeneous and heterogeneous, should produce the same results. If the particles are large, the heterogeneous (or microscopic) approach becomes more applicable than the homogeneous approach with appropriate correction for the current at a particle. With the conditions shown in the footnote * when the particle radius is 0.1 cm, the potential drop between both ends of the particle is 0.02 V. The current density at the bottom end is 78% of the current density at the top end. Corresponding correction for the current at a particle is possible in the heterogeneous model, too. However, the existence of the contact resistance and its dependence on the nature of contact are introduced in the heterogeneous model realistically. (A nonuniform electrode resistance could be incorporated into the homogeneous model as a continuous function.) Basically, the heterogeneous approach is a different type of treatment of the same system and offers a method by which the contact resistance is calculated. Once the contact resistance has been estimated, there is no real difference in both approaches, except the expression of differential equations (homogeneous) or summation equations (heterogeneous). An advantage of the heterogeneous approach includes the ability to take into account the contact resistance caused by the surface films which are the origin of an important contribution to the *IR* drop throughout the electrode phase.

5. Conclusion

A microscopic heterogeneous model for a packed bed electrode was established for the case that oxide films at the particle-particle contacts are significant. With reasonable selection of constants, the model can predict the current at a packed bed electrode as a function of the applied potential, particle radius, and bed length.

The finite resistance of the electrode phase decreases the total current in the packed bed electrode, but leads to a more uniform overpotential distribution than in a packed bed in which contact resistances through the electrode phase are neglected.

Acknowledgements

This work was funded by the Department of Energy Office of Technology Development (Office of Environmental Management), through the Efficient Separations and Processing Integrated Program, Teresa B. Fryberger, Headquarters program Manager, and Allison M. Blackman, Cognizant Technical Program Officer. The Welch Foundation supported the publication costs of this article. Throughout the work, discussion with Dr D. Hobbs and Dr R. White took place and contributed significantly to the success of the investigation.

References

[1] I. C. Agarwal, A. M. Rochon, H. D. Gesser and A. B. Sparling, *Water Res.* **18** (1984) 227.
[2] D. Golub and Y. Oren, *J. Appl. Electrochem.* **19** (1989) 311.
[3] M. Matlosz and J. Newman, *J. Electrochem. Soc.* **133** (1986) 1850.
[4] Y. Sun, W. Xu and K. Scott, *Electrochim. Acta* **38** (1993) 1753.
[5] J. C. Card, S. E. Lyke and S. H. Langer, *J. Appl. Electrochem.* **20** (1990) 269.
[6] S. G. Chen, T. Wen and J. H. P. Utley, *ibid.* **22** (1992) 43.
[7] J. Nanzer, S. Langlois and F. Coeuret, *Ibid.* **23** (1993) 471, 477.
[8] P. A. Dykstra, G. H. Kelsall, X. Liu and A. C. C. Tseung, *ibid.* **19** (1989) 697.
[9] B. E. El- Anadouli, M. M. Khader, M. M. Saleh and B. G. Ateya *ibid.* **21** (1991) 166.
[10] J. Qi and R. F. Savinell, *ibid.* **23** (1993) 873, 887.
[11] J. A, McIntyre, *Electrochem Soc. Interface* **4(1)** (1995) 29.
[12] A. K. P Chu, M. Fleischmann and G. J. Hills, *J. Appl. Electrochem.* **4** (1974) 323.
[13] R. Alkire and P. K. Ng, *J. Electrochem. Soc.* **124** (1977) 1220.
[14] G. Kreysa and E. Heitz, *Electrochim. Acta* **20** (1975) 919.
[15] P. Fedkiw and J. Newman, *AlChE J.* **25** (1979) 1077.
[16] C. Y. Yuh and J. R. Selman, *Chem. Eng. Commun.* **38** (1985) 135.
[17] S. E. Lyke and S. H. Langer, *J. Electrochem. Soc.* **138** (1991) 2327.
[18] B. E. ElAnadouli and B. G. Ateya, *J Appl. Electrochem.* **22** (1992) 277.
[19] K. Scott, Y. P. Sun and W. Xu, *in* 'Topics in Electrochemical Engineering' (edited by J. Newman and R. E. White), **PV94–22**, The Electrochemical Society Proceedings Series, Pennington, NJ (1994), p. 337.
[20] J. S. Newman and C. W. Tobias, *J. Electrochem. Soc.* **109** (1962) 1183.
[21] J. O'M. Bockris and J. Kim, *J. Electrochem. Soc.*, in press.
[22] F. A. L. Dullien, 'Porous Media Fluid Transport and Pore Structure', 2nd edn, Academic Press, San Diego (1992), p. 73.
[23] V. M. M. Lobo and J. L. Quaresma, 'Handbook of Electrolyte Solution', Part B, Elsevier, New York (1989), p.1778, p.1781 and p.1803.
[24] D. A. G. Bruggeman, *Ann. Phy. (Germany)* **24** (1935) 636.
[25] M. S. El- Genk, D. Louie, E. Bergeron and D. Nfitchell, *in* 'Heat Transfer' (edited by N. M. Farukhi), **79**, AlChE Symposium Series 225, New York, (1983) p.256.
[26] F. P. Bowen and D. Tabor, 'The Friction and Lubrication of Solids', Clarendon Press, Oxford (1950).
[27] R. Holm, 'Electric Contacts', Almquist & Wiksells, Sweden (1946).
[28] A. J. Arvia and D. Posadas, *in* 'Encyclopedia of Electrochemistry of the Elements' vol. 3, (edited by A. J. Bard), Marcel Dekker, New York (1975) p.211.
[29] T. P. Barrera and K. Nobe, *in*, 'Topics in Electrochemical Engineering' (edited by J. Newman and R. E. White), **PV94–22**, The Electrochemical Society Proceedings Series, Pennington, NJ (1994), p.229.
[30] J. O'M. Bockris, A. K. N. Reddy and B. Rao, *J. Electrochem. Soc.* **113** (1966) 1133.
[31] J. Kim, PhD dissertation, Texas A&M University (1996).
[32] S. Trasatti and G. Lodi, *in* 'Electrodes of Conductive Metallic Oxides' (edited by S. Trasatti), Elsevier, New York (1980), p.301.
[33] J. O'M. Bockris and S. D. Argade, *J. Chem. Phys.* **50** (1969) 1622.
[34] E. M. Lazarova, *Elektrokhimiya* **14** (1978) 1300.
[35] K. Ogawa, S. Yoshikawa and J. S. Lee, *J. Chem. Eng. (Japan)* **24** (1991) 788.
[36] D. N. Bennion and J. Newman, *J. Appl. Electrochem.* **2** (1972) 113.

Appendix A: Evaluation of overpotential difference between two neighbouring slabs.

The current at each slab is designated as $I_1, I_2, \cdots, I_N$ (see Fig. 8) where the suffix indicates the order of numbering from the bottom of the packed bed. The overpotential at each slab is also designated as $\eta_1, \eta_2, \cdots, \eta_N$. From the two top slabs, Nth and $(N-1)$th slabs, the following relation has to be observed:

$$\eta_{N-1} = \eta_N + (I_T - I_N)R_s - I_N R_m \tag{A1}$$

where I_N is the current through the particle contact and $(I_T - I_N)$ is the current in the solution phase from Nth slab to $(N-1)$th slab, and R_s and R_m are the resistance of the solution phase and the particle contact resistance between the two slabs, respectively. The overpotential at the $(N-2)$th slab is then

$$\eta_{N-2} = \eta_{N-1} + (I_T - I_N - I_{N-1})R_s - (I_N + I_{N-1})R_m \tag{A2}$$

A generalized form is

$$\eta_{n-1} = \eta_n + (I_T - I_N - I_{N-1} - \ldots - I_n)R_s - (I_N + I_{N-1} + \ldots + I_n)R_m \tag{A3}$$

Since

$$I_T = I_N + I_{N-1} + \ldots + I_n + \ldots + I_1 \tag{A4}$$

the general form is simplified to be

$$\eta_{n-1} = \eta_n + \sum_{n=1}^{n-1} I_n R_s - \left(I_T - \sum_{n=1}^{n-1} I_n\right) R_m \tag{A5}$$

then

$$\eta_n = \eta_{n-1} - \sum_{n=1}^{n-1} I_n R_s + \left(I_T - \sum_{n=1}^{n-1} I_n\right) R_m \tag{7}$$

Appendix B: Equivalence of Equation 25 to the expression by Chu *et al.*

The expression of Chu *et al.* for the current under mass transfer control is

$$I = n\,Fau \int_{x=0}^{L} C_x \mathrm{d}x = n\,Fau\,C_L\left[1 - \exp\left(-\frac{DA\varepsilon L}{\delta u}\right)\right] \tag{A6}$$

where a is the cross-sectional area of the bed, u is the flow rate, C_L is the inlet concentration at the top of the bed, D is the diffusion coefficient, δ is the diffusion layer thickness, A is the specific area per unit volume of the bed, ε is the voidage and L is the bed length. Equation 25 is rewritten as

$$I_T = \frac{2\pi anFD}{\sqrt{3}\ \delta_{PBE}} \int_{m=0}^{L/2r} C_m \mathrm{d}m \tag{A7}$$

From Equations 21 and 24,

$$\frac{\mathrm{d}C_m}{\mathrm{d}m} = \frac{2\pi D\varepsilon}{\sqrt{3}\ \delta_{PBE} u} C_m$$

$$C_m = \varepsilon C_L \exp\left[\frac{2\pi D\varepsilon}{\sqrt{3}\ \delta_{PBE} u}\left(m - \frac{L}{2r}\right)\right] \tag{A8}$$

Putting Equation A8 into A7 gives

$$I_T = nFauC_L\left[1 - \exp\left(-\frac{\pi D\varepsilon L}{\sqrt{3}\ \delta_{PBE} ur}\right)\right] \tag{A9}$$

which becomes same as Equation A6 when $A = \pi/r\sqrt{3}$. Since A is defined as the specific area per unit volume, AaL is the area of a packed bed where a and L are the cross-sectional area and the length of the bed (see Fig. 7). There are $L/2r$ slabs in the bed and $a/r^2 2\sqrt{3}$ particles in a slab. The area of the bed is then $(L/2r) \times (a/r^2 2\sqrt{3}) \times 4\pi r^2 = AaL$; thus, $A = \pi/r\sqrt{3}$.